Signatures of right-handed Majorana neutrinos and gauge bosons in $e\gamma$ collisions

Nikolai Romanenko
Ottawa-Carleton Institute for Physics, Department of Physics, Carleton University, Ottawa, Canada K1S 5B6
(Received 2 October 2002; published 18 February 2003)

The process $e^- \gamma \to e^+ W_R^- W_R^-$ is studied in the framework of the left-right symmetric model. It is shown that this reaction and $e^- \gamma \to l^+ W_R^- W_R^-$ for the arbitrary final lepton are likely to be discovered at the CLIC collider. For a relatively light doubly charged Higgs boson its mass does not have much influence on the discovery potential, while for heavier values the probability of the reaction increases.

DOI: 10.1103/PhysRevD.67.033002 PACS number(s): 12.15.Ji, 12.60.Cn, 14.80.Cp

I. INTRODUCTION

Majorana neutrino masses arise naturally in many extensions of the standard model (SM) such as singlet Majorana mass model [1], Higgs triplet model [2], or left-right symmetric model (LRM) [3]. One of the main sources of their popularity comes from the so-called see-saw mechanism [1] where the left-handed neutrinos turn out to be light due to the corresponding right-handed neutrinos being heavy. The LRM can easily include heavy right-handed Majorana neutrinos and the see-saw mechanism since it has a heavy mass scale determined by the $SU(2)_R$ symmetry breaking. In this case the LRM contains a triplet Higgs field with hypercharge $Y=2$ [3].

The theory with massive Majorana neutrinos, especially with heavy ones, allows a variety of processes violating lepton number conservation. They provide beautiful signatures which can be tested at various collider options. Estimates of the discovery probability for heavy Majorana neutrinos at the CERN Large Hadron Collider (LHC) were done in [4] and for electron-positron colliders in [5]. An electron-electron collider provides a specific and very useful option for Majorana neutrino search, the so-called ''the inverse double-β decay'' process. Together with some associated processes, it was studied in [6]. For the electron-proton option of the DESY *ep* Collider HERA, Majorana neutrino production was studied in [7], for a Very Large Hadron Collider (VLHC) in [8], and for an electron-photon collider in [9].

All these estimates should be combined with the restrictions obtained from the neutrinoless double β decay [10], the well-known low-energy lepton-number violating process. The resulting numbers essentially depend on the chirality of neutrinos and on the bosonic sector of the model. For example, limitations from double β decay in the framework of the standard model (SM) bosonic sector yield an upper bound on the effective electron neutrino mass $\langle m_{\nu_e} \rangle \leqslant 0.2$ eV, while for the case of the LRM heavy right-handed neutrinos are allowed with the lower bound depending on the mass of the right-handed gauge boson [10].

In this paper we will concentrate on the electron-photon collider option. We will study the signatures for heavy right-handed Majorana neutrinos in the process $e^- \gamma \to e^+ W_R^- W_R^-$. This process is analogous to the one considered in [9] for the left-handed gauge bosons. However, since the current limitations for W_R masses are relatively strict and imply $M_{W_R} \geqslant 700$ GeV [11], the above-mentioned process with two final state W_R's is likely to be discovered only at the collider machines with very high center of mass energies. The CERN Linear Collider (CLIC) proposal [12] is anticipated to provide $\sqrt{s}=3,5$, and 8 TeV energies, appropriate for the process chosen. We assume the integrated luminosity of $L=500$ fb^{-1}. Final state W_R bosons are expected to decay mostly into quark jets and hence to be identified through the quark jets with an appropriate invariant mass. Due to presence of the final state positron, the process has no SM background.

In the next section we will briefly discuss the main features of the LRM and discuss some phenomenological constraints on the parameters of this model.

II. THE MODEL

In this section we give a brief description of the LRM. For more detailed reference one can refer to [3]. The gauge symmetry of the LRM extends the SM gauge group to $SU(2)_L \times SU(2)_R \times U(1)_{B-L}$. The fermionic sector contains, in addition to SM particles, right-handed neutrinos: one specie for each generation. Quarks and leptons transform under the gauge group as follows:

$$Q_{iL}=\begin{bmatrix} u \\ d \end{bmatrix}_{iL} = \left(2,1,\frac{1}{3}\right); \quad Q_{iR}=\begin{bmatrix} u \\ d \end{bmatrix}_{iR} = \left(1,2,\frac{1}{3}\right), \tag{1}$$

$$\Psi_{iL}=\begin{bmatrix} \nu \\ e \end{bmatrix}_{iL} = (2,1,-1); \quad \Psi_{iR}=\begin{bmatrix} \nu \\ e \end{bmatrix}_{iR} = (1,2,-1), \tag{2}$$

where i is the flavor index, L and R denote left-handed and right-handed chirality, Q and Ψ stand for quark and lepton wave functions, respectively. The gauge sector includes right-handed gauge bosons W_R and Z_R in addition to SM gauge bosons. The greatest extension has to be done for the scalar sector. In order to supply quarks and leptons with masses one needs the Higgs bidoublet field with the following quantum numbers:

$$\Phi=\begin{pmatrix} \phi_1^0 & \phi_1^+ \\ \phi_2^- & \phi_2^0 \end{pmatrix} = (2,2^*,0),$$

and with the following vacuum expectation value (VEV)

$$\langle\Phi\rangle=\frac{1}{\sqrt{2}}\begin{pmatrix}k_1 & 0\\ 0 & k_2\end{pmatrix}.$$

In addition to this, another Higgs field with nonzero $B-L$ quantum number is necessary in order to provide symmetry breaking of $SU(2)_L\times SU(2)_R\times U(1)_{B-L}$ to the SM gauge group. The most popular way to do it also gives rise to Majorana masses for neutrinos: this way is to introduce a Higgs triplet field

$$\Delta_R=\begin{pmatrix}\Delta_R^+/\sqrt{2} & \Delta_R^{++}\\ \Delta_R^0 & -\Delta_R^+/\sqrt{2}\end{pmatrix}=(1,3,2) \tag{3}$$

with the vacuum expectation value:

$$\langle\Delta_R\rangle=\frac{1}{\sqrt{2}}\begin{pmatrix}0 & 0\\ v_R & 0\end{pmatrix}. \tag{4}$$

For an explicit (manifest) $L\leftrightarrow R$ symmetry, the corresponding left-handed Higgs-Majoron field should also be introduced:

$$\Delta_L=\begin{pmatrix}\Delta_L^+/\sqrt{2} & \Delta_L^{++}\\ \Delta_L^0 & -\Delta_L^+/\sqrt{2}\end{pmatrix}=(3,1,2) \tag{5}$$

with the vacuum expectation value:

$$\langle\Delta_L\rangle=\frac{1}{\sqrt{2}}\begin{pmatrix}0 & 0\\ v_L & 0\end{pmatrix}. \tag{6}$$

The Yukawa interactions of the Higgs triplets with fermions in the model read:

$$-\mathcal{L}_{Yuk}=ih_{R,ll'}\Psi_{lR}^T C\sigma_2\Delta_R\Psi_{l'R}+ih_{L,ll'}\Psi_{,L}^T C\sigma_2\Delta_L\Psi_{l'L}+\text{H.c.}, \tag{7}$$

where l,l' are flavor indices, these interactions yield Majorana mass to neutrinos and are relevant to the process studied in this paper. Since left-handed neutrinos are practically massless one expects v_L to be small, while the value of v_R provides natural scale for the right-handed neutrino masses. After ignoring possible mixing between lepton families the masses of right-handed Majorana neutrinos are given by $m_{Ri}=\sqrt{2}h_{R,ii}v_R$.

For further considerations I will choose $v_L=k_2=0$, this condition being compatible with phenomenological limits [14]. The gauge couplings for the left-handed and right-handed gauge groups are set equal, $g_L=g_R$.

Present phenomenological bounds on the triplet Yukawa couplings $h_{ll'}$ were discussed in [13], they satisfy $h/M_{\Delta^{++}}<0.44\ \text{TeV}^{-1}$. The limit on the masses of right-handed gauge bosons is $M_{W_R}>700$ GeV [11].

III. CALCULATIONS AND RESULTS

Nine Feynman diagrams are involved in the $e^-\gamma\to e^+W_RW_R$ process, see Fig. 1. Diagrams 1–4 do not contain doubly charged Higgs field Δ^{--} and correspond to the diagrams considered in [9], with the proper change of chiralities of particles. Diagrams 5–9 involve virtual Δ^{--}. Using the CALCUL technique [15] we obtained the expressions for chirality amplitudes presented in the Appendix. Alternatively, the expressions for square matrix elements were obtained by means of the COMPHEP package [16]. We have checked the consistency of our results with [9]: if the value of the charged boson mass is set to 80 GeV, diagrams with doubly charged Higgs boson are neglected and the initial photon energy is fixed, the results are the same as in Fig. 2 of [9].

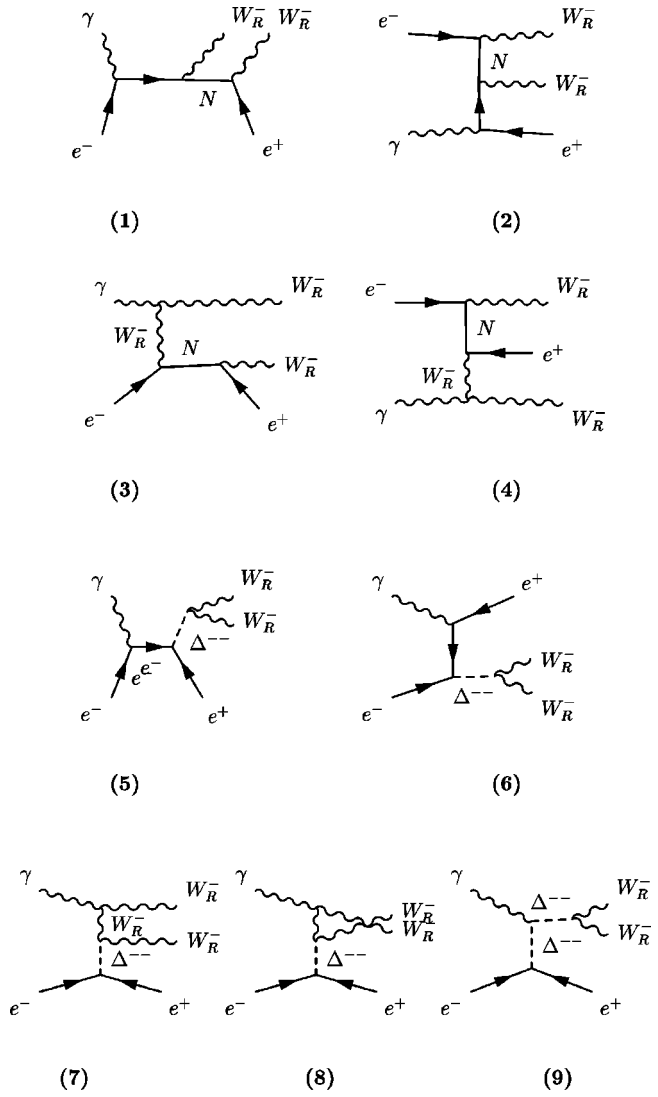

FIG. 1. The Feynman diagrams for the $e^-\gamma\to e^+W_RW_R$ process.

In contrast to [9] we have used the backscattered laser photon spectrum [17] for the initial state photon so that the cross section of the process is described by convoluting the fixed photon energy cross section with this spectrum:

$$\sigma=\int dx f_{\gamma/e}(x,\sqrt{s}/2)\ \ \hat{\sigma}(e^-\gamma\to e^+W_R^-W_R^-). \tag{8}$$

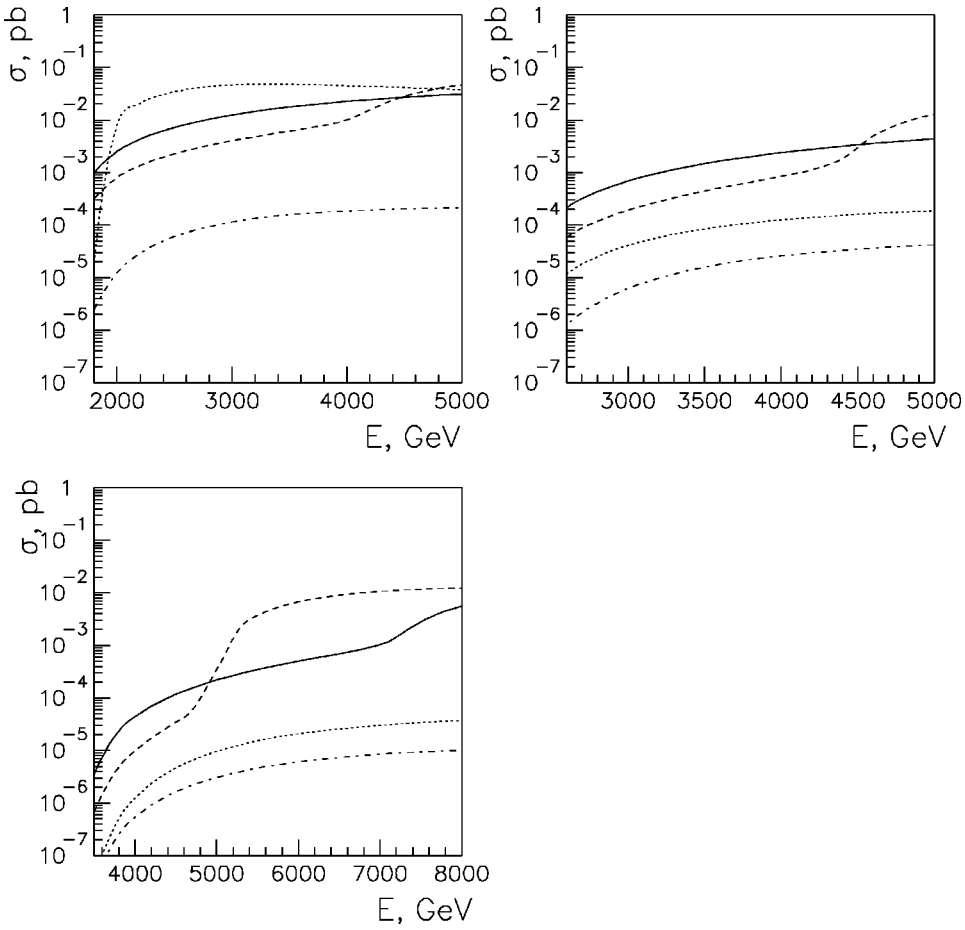

FIG. 2. The cross section $\sigma(e^- \gamma \to e^+ W_R^- W_R^-)$ as a function of $\sqrt{s_{ee}}$. The mass of the doubly charged Higgs is $M_{\Delta_{++}} = 600$ GeV. $M_{W_R} = 700$, 1000, and 1500 GeV for upper left, upper right, and lower paints, correspondingly. In all three cases the solid line is for neutrino mass $M_N = 5$ TeV, the long-dashed line for $M_N = 3$ TeV, the short-dashed for $M_N = 1$ TeV, and the dashed-dotted line for $M_N = 500$ GeV.

The following final state cuts were applied: $|\cos\theta_{1f}| < 0.9$, $E_{e^+} > 10$ GeV, these cuts are based on the detector considerations.

In Fig. 2 the cross section of the process is shown as a function of electron-positron collision energy $\sqrt{s_{ee}}$. In all three paints of Fig. 2 the mass of the doubly charged Higgs boson is 600 GeV, while the masses of the right-handed gauge boson are $M_{W_R} = 700$, 1000, and 1500 GeV correspondingly. Each of the paints contains four curves for different values of Majorana neutrino mass: $M_N = 5$ TeV (solid line), $M_N = 3$ TeV (long-dashed line), $M_N = 1$ TeV (short-dashed line), and $M_N = 500$ GeV (dash-dotted line). Thresholds of the curves are due to the Majorana neutrino propagator pole:

$$\Pi(p_1 + p_2 - p_4 - p_5, M_N, \Gamma_N) = \frac{1}{s + M_W^2 - M_N^2 - 2(p_1 + p_2)(p_4 + p_5) + iM_N\Gamma_N}.$$

Figure 3 shows the effects of Majorana neutrino and doubly charged Higgs widths in the propagators of the amplitudes. In that figure the right-handed boson mass is 1 TeV, $\sqrt{s_{ee}} = 5$ TeV. The dashed-dotted line represents the cross section of the process as a function of Majorana neutrino mass with the constant decay widths $\Gamma_N = \Gamma_{\Delta^{++}} = 10$ GeV.

In general, the decay width for heavy Majorana neutrino $N \to W^\pm l^\mp$ (where l stands for massless lepton) is given by:

$$\Gamma_N = \frac{g^2}{(32\pi M_N^3 M_W^2)}(M_N^2 - M_W^2)(M_N^4 + M_N^2 \cdot M_W^2 - 2M_W^4) \tag{9}$$

(in the case when $M_{W_R} > M_N$ the above-mentioned mode is closed but there may exist decay modes to left-handed bosons through some mixing effects). As for the decay modes of the doubly charged Higgs boson it is useful to take two fermion decays ($\Delta^{++} \to l^+ l^+$) into account explicitly:

$$\Gamma_{\Delta^{++} \to l^+ l^+} = \frac{1}{8\pi} h_{ll}^2 M_{\Delta^{++}} \tag{10}$$

(here h_{ll} stands for the Yukawa coupling to lepton l) while leaving possible bosonic decay width as a free phenomenological parameter (for a more detailed discussion see [13]):

$$\Gamma_{\Delta^{++}} = \Gamma_b + \Gamma_f. \tag{11}$$

In the following calculations we have chosen $\Gamma_b = 10$ GeV. The solid line in Fig. 3 corresponds to the mass dependent widths Γ_N and $\Gamma_{\Delta^{++}}$ according to Eqs. (9) and (11). However, Δ^{++} width does not play much of a role in the estimates of the cross section: the dashed line in Fig. 3 [Γ_N as in Eq. (9), $\Gamma_{\Delta^{++}} = 10$ GeV] is completely invisible since it co-

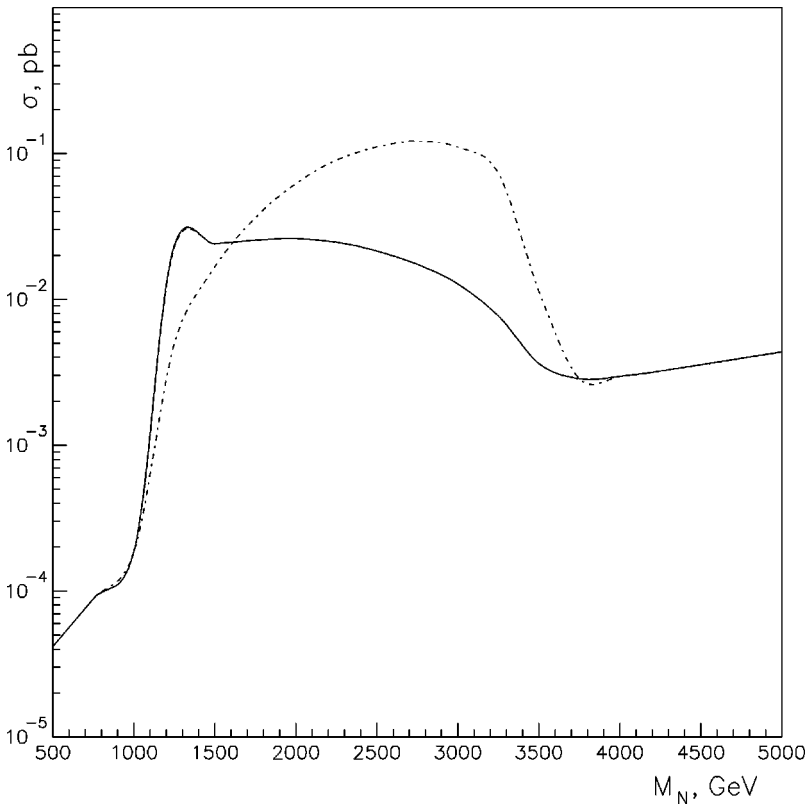

FIG. 3. The cross section $\sigma(e^- \gamma \to e^+ W_R^- W_R^-)$ as a function of right-handed Majorana neutrino mass for $M_{W_R}=1$ TeV, $\sqrt{s_{ee}}=5$ TeV. The dash-dotted line is for constant neutrino and doubly charged higgs widths $\Gamma_N=\Gamma_{\Delta^{++}}=10$ GeV, the solid line is for realistic, mass dependent widths. The dashed line (completely coinciding with the solid one) is for $\Gamma_{\Delta^{++}}=10$ GeV and realistic Γ_N.

incides with the solid one. As in [9] the curves reach their highest values within a certain range of M_N masses (''peak-like'' behavior), though they do not decrease much (as in [9]) when M_N is above this range, the latter happens due to effects of the doubly charged Higgs boson. In general one can state that the increase of Majorana neutrino's width decreases the cross section of the process in the mass range when the cross section has ''peak-like'' behavior and has not much influence on the cross section away from that ''peak.''

Figures 4 and 5 represent the cross section as a function of mass of the right-handed boson for the three CLIC options: $\sqrt{s_{ee}}=3$, 5, and 8 TeV. In Fig. 4 all the effects of doubly charged Higgs boson are neglected (only diagrams 1–4 are taken into account, or, equivalently, mass of the doubly charged boson can be set infinitely large). In Fig. 5 $M_{\Delta^{++}}=600$ GeV and one can see that these curves look similar to those of Fig. 4. Threshold behavior at $M_W \sim M_N$ can be explained by the change of sign of propagator terms (diagrams 2 and 4):

$$\Pi(p_1-p_4-p_5,M_N,\Gamma_N) = \frac{1}{M_W^2-M_N^2-2p_1\cdot(p_4+p_5)+iM_N\Gamma_N}.$$

In order to study the influence of $M_{\Delta^{++}}$ on the cross section Fig. 6 shows the discovery limits of the reaction $e^- \gamma \to e^+ W_R^- W_R^-$ in the $M_N - M_{\Delta^{++}}$ plane for the $\sqrt{s_{ee}}=5$ TeV and $M_{W_R}=1$ TeV. Final state W_R are assumed to decay into light quark jets (third generation excluded), and the four-quark efficiency is taken to be 85% and purity 80%, with the efficiency for final e^+90% [18]. The contour levels in the figure are drawn at 63%, 95%, and 99% probability of the reaction discovery (1, 3, and 4.6 events per year with the anticipated luminosity). The excluded region lies below the curves because of the lower limit on the Majorona mass of the neutrino. One can see the threshold at $M_{\Delta^{++}}=2M_{W_R}$, it happens due to the pole in the Δ^{++} propagator which gets involved in the integration over final states. Above this threshold, the reaction $e^- \gamma \to e^+ W_R^- W_R^-$ is observable even for the very low value of Majorana neutrino mass, however, even below this threshold the reaction remains observable for neutrino masses above 500 GeV. This means that effects of doubly charged Higgs mass are not important for the reaction studied. In further calculations we set $M_{\Delta^{++}}=600$ GeV which keeps the Δ^{++} propagator off-shell for realistic values of doubly charged boson masses (and hence the reaction is studied in a more conservative regime, without possible Δ^{++} pole enhancement).

It is also important to state here that the process under study takes place only due to the Majorana mass of the neutrinos, in other words all amplitudes presented in the Appendix are proportional to

$$A^n \sim M_N \cdot a^n(M_N) \tag{12}$$

and vanish for the case of massless neutrinos. They can be generalized for the general case of right-handed neutrino mixings:

$$A^n \sim \sum_i U_{ei}^2 \cdot M_{Ni} \cdot a^n(M_{Ni}). \tag{13}$$

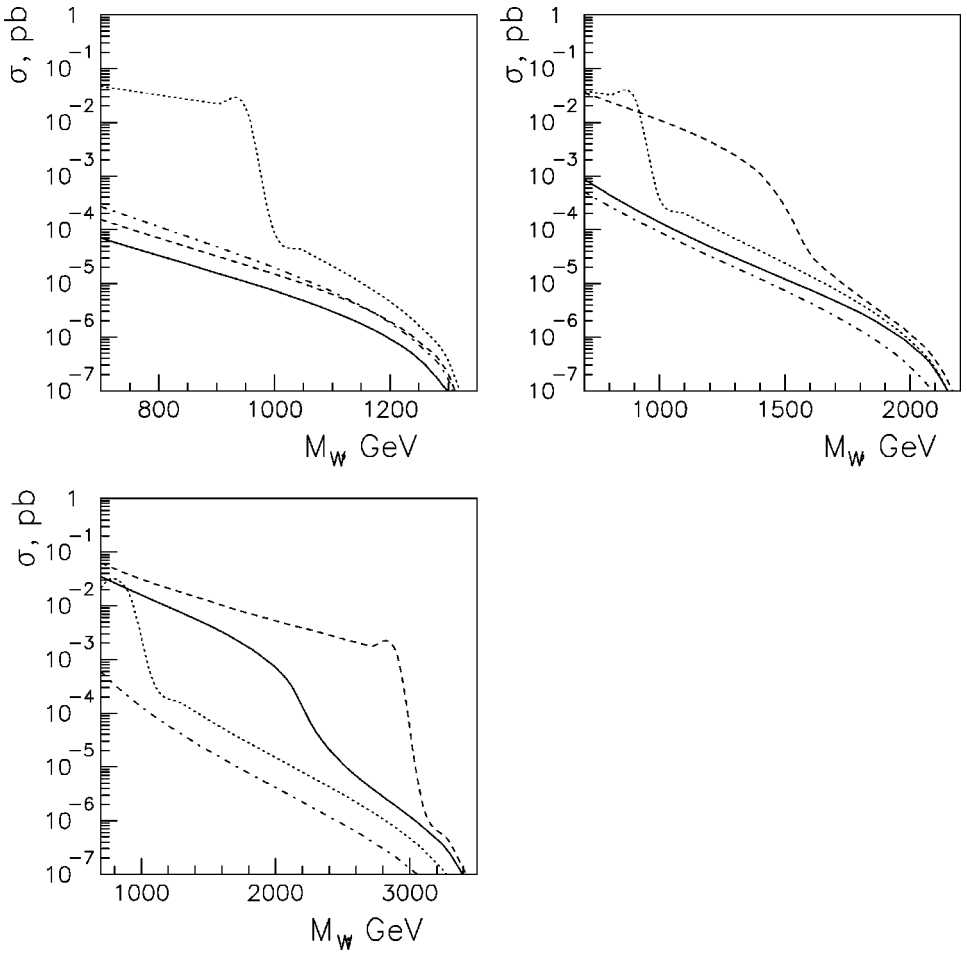

FIG. 4. The cross section $\sigma(e^- \gamma \to e^+ W_R^- W_R^-)$ as a function of M_{W_R}. Diagrams with doubly charged Higgs boson are neglected. $\sqrt{s_{ee}}=3$, 5, and 8 TeV for upper left, upper right, and lower paints, correspondingly. In all three cases the solid line is for neutrino mass $M_N=5$ TeV, the long-dashed line for $M_N=3$ TeV, the short-dashed for $M_N=1$ TeV, and the dashed-dotted line for $M_N=500$ GeV.

From Figs. 3, 5, and 6 it is possible to conclude that for neutrino masses $M_N<M_{W_R}$ the cross section of the process essentially decreases and at some point $M_N\sim 500$ GeV the process becomes invisible for the case of $M_{\Delta^{++}}<2M_{W_R}$. If the latter condition does not hold the cross section still turns off but at the lower values of M_N. Hence, if the right-handed mass spectrum is such that only one neutrino mass state is heavy enough to be ''visible'' (let us denote it as m_{heavy}), the results presented may be generalized for the process $e^- \gamma \to l^+ W_R W_R$ with muon or τ-lepton in the final state. Defining in the standard way the effective neutrino masses:

$$\langle m_{ik}\rangle = \sum_j U_{ij}\cdot U_{kj} m_j$$

one can treat all the figures as referring to an arbitrary final lepton with the following changes:

$$\sigma(e^- \gamma \to e^+ W_R^- W_R^-, M_N) \to \frac{m_{\text{heavy}}^2}{\langle m_{el}\rangle^2}\sigma(e^- \gamma \to l^+ W_R^- W_R^-, m_{\text{heavy}}), \quad (14)$$

$$M_N \to m_{\text{heavy}}.$$

Finally, in Fig. 7 are depicted the discovery limits for the studied process in the $M_N - M_{W_R}$ plane for CLIC options $\sqrt{s_{ee}}=3$ TeV (a), $\sqrt{s_{ee}}=5$ TeV (b), and $\sqrt{s_{ee}}=8$ TeV (c). As indicated $M_{\Delta^{++}}$ is set at 600 GeV. The treatment of the final W_R decays is the same as for Fig. 6. The contour levels in the figure are drawn at 63%, 95%, and 99% probability of the reaction discovery (1, 3, and 4.6 events per year with the anticipated luminosity). The excluded region is above the curves. It is possible to state that the reaction $e^- \gamma \to e^+ W_R^- W_R^-$ will be observed for heavy Majorana neutrinos, whose masses may essentially exceed straightforward discovery limit ($M_N > \sqrt{s_{ee}}$) for reasonable values of right-handed charged bosons. The corresponding lower limit on M_N increases with the increase of charged boson mass, and the ''resonance-like'' behavior of the contour-levels occurs due to interplay of M_N and M_{W_R} in the propagators of diagrams 2 and 4 (see comments to Figs. 4 and 5).

We do not present here the angular distributions of the final lepton since—in complete accordance with [9]—the shape of these distributions is nonuniversal and is governed by the interplay between $\sqrt{s}$ and M_N.

IV. SUMMARY

The LR model with heavy Majorana neutrinos is one of the most natural and popular extensions of the SM. Obser-

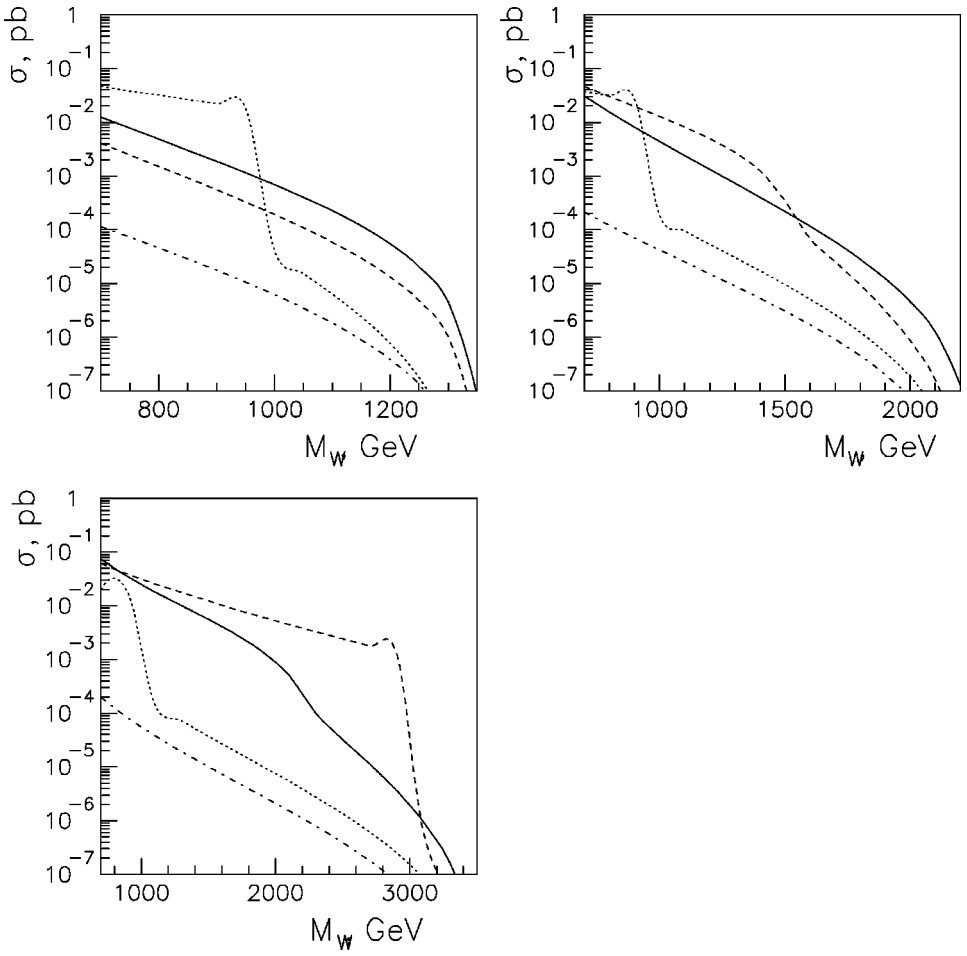

FIG. 5. The cross section $\sigma(e^- \gamma \to e^+ W_R^- W_R^-)$ as a function of M_{W_R}. The mass of the doubly charged Higgs is $M_{\Delta_{++}} = 600$ GeV. $\sqrt{s_{ee}} = 3$, 5, and 8 TeV for upper left, upper right, and lower paints, correspondingly. In all three cases the solid line is for neutrino mass $M_N = 5$ TeV, the long-dashed line for $M_N = 3$ TeV, the short-dashed for $M_N = 1$ TeV, and the dashed-dotted line for $M_N = 500$ GeV.

vation of right-handed gauge bosons, Majorana neutrinos, and triplet Higgs bosons are necessary steps for the confirmation of this theory. The reaction $e^- \gamma \to e^+ W_R^- W_R^-$ can be discovered at CLIC for a reasonable range of values of LR model parameters, providing a good test of lepton number violation in the LR model. The reaction would be a serious manifestation of a heavy Majorana neutrino. It will be observable for realistic mass values of right-handed bosons in the neutrino mass range $M_N \sim \sqrt{s}$ and even well above limits for direct N production ($M_N > \sqrt{s}$). Discovery limits on M_N depend on the corresponding value of M_{W_R} and are very weakly dependent on the doubly charged boson mass. However, extra heavy doubly charged Higgs ($M_{\Delta^{++}} > 2M_{W_R}$) can increase the probability of the reaction. If the right-handed Majorana neutrino spectrum has only one heavy eigenvalue, all the results can be applied to the process $e^- \gamma \to l^+ W_R W_R$ with the arbitrary lepton in the final state.

ACKNOWLEDGMENTS

This research was supported in part by the Natural Sciences and Engineering Research Council of Canada and partially supported by RFFI Grant 01-02-17152 (Russian Fund of Fundamental Investigations) and by INTAS grant 2000-587. I would like to thank Professor Pat Kalyniak for careful reading of the manuscript and Professor Steve Godfrey and Professor Richard Hemingway for useful discussions.

APPENDIX

We present here helicity amplitudes for Feynman diagrams 1–9 of Fig. 1. I use the following notations for particle momenta: p_1, p_2 are the incident electron and photon moments correspondingly. p_3 stands for outgoing positron (positively charged lepton), p_{45}, p_{67} are, correspondingly, momenta of outgoing right-handed bosons, where $p_{ij} = p_i + p_j$ and p_i, p_j are four-momenta of massless fermions (see the CALCUL technique of massive gauge bosons representation), k is the photon CALCUL representation vector [15]. The gauge couplings are e-electrical charge, g_R right-handed SU(2) gauge coupling. M_N, Γ_N, M_W, Γ_W, M_Δ, and Γ_Δ denote the masses and widths of right-handed Majorana neutrino, charged gauge boson, and doubly charged Higgs correspondingly. The propagator function is defined as follows:

$$\Pi(k,M,\Gamma) = \frac{1}{k^2 - M^2 + iM\Gamma}.$$

The upper index of the amplitudes denotes the number of the corresponding Feynman diagram, the lower index (L, R) denotes the chirality of the incoming photon.

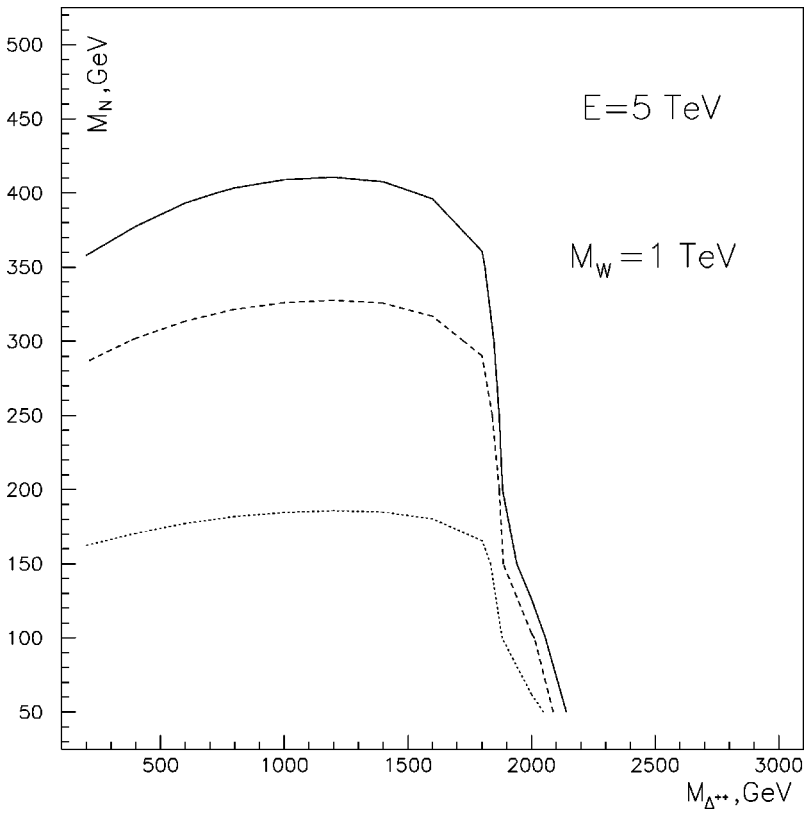

FIG. 6. The contour levels in the M_N–$M_{\Delta^{++}}$ plane that correspond to 99% (solid line), 95% (long-dashed line), and 63% (short-dashed line) probability of the discovery level (4.6, 3, and 1 event) for $\sqrt{s}=5$ TeV, $M_{W_R}=1$ TeV.

$$A_\lambda^1=\frac{ieg_R^2}{2}\cdot\frac{1}{\sqrt{4kp_2}}\cdot\Pi(p_1+p_2,0,0)\cdot\Pi(p_1+p_2-p_{45},M_N,\Gamma_N)\cdot\hat{A}_\lambda^1+(45\leftrightarrow 67), \tag{A1}$$

$$\hat{A}_L^1=8M_N\cdot s(p_1,k)t(p_2,p_1)s(p_1,p_4)t(p_5,p_7)s(p_6,p_3),$$

$$\hat{A}_R^1=8M_N\cdot s(p_1,p_2)[t(k,p_1)s(p_1,p_4)+t(k,p_2)s(p_2,p_4)]t(p_5,p_7)s(p_6,p_3).$$

$$A_\lambda^2=\frac{ieg_R^2}{2}\cdot\frac{1}{\sqrt{4kp_2}}\cdot\Pi(p_3-p_2,0,0)\cdot\Pi(p_1-p_{45},M_N,\Gamma_N)\cdot\hat{A}_\lambda^2+(45\leftrightarrow 67), \tag{A2}$$

$$\hat{A}_L^2=-8M_N s(p_1,p_4)t(p_5,p_7)s(p_6,p_3)t(p_3,p_2)s(k,p_3),$$

$$\hat{A}_R^2=-8M_N s(p_1,p_4)t(p_5,p_7)[s(p_6,p_3)t(p_3,k)s(p_2,p_3)-s(p_6,p_2)t(p_2,k)s(p_2,p_3)].$$

$$A_\lambda^3=\frac{ieg_R^2}{2}\cdot\frac{1}{\sqrt{4kp_2}}\cdot\Pi(p_1+p_2-p_{45},M_N,\Gamma_N)\cdot\Pi(p_{45}-p_2,M_W,0)\cdot\hat{A}_\lambda^3+(45\leftrightarrow 67), \tag{A3}$$

$$\begin{aligned}\hat{A}_L^3=&-8M_N s(p_6,p_3)\{s(p_1,p_2)t(p_2,p_7)s(p_4,k)t(p_2,p_5)\\&-s(p_1,p_4)t(p_5,p_7)[t(p_2,p_4)s(p_4,k)+t(p_2,p_5)s(p_5,k)]-s(p_4,p_2)t(p_2,p_5)s(p_1,k)t(p_2,p_7)\},\end{aligned}$$

$$\begin{aligned}\hat{A}_R^3=&-8M_N s(p_6,p_3)\{s(p_1,p_2)t(p_2,p_7)s(p_4,p_2)t(k,p_5)\\&-s(p_1,p_4)t(p_5,p_7)[s(p_2,p_4)t(p_4,k)+s(p_2,p_5)t(p_5,k)]-s(p_4,p_2)t(p_2,p_5)s(p_1,p_2)t(k,p_7)\}.\end{aligned}$$

$$A_\lambda^4=\frac{ieg_R^2}{2}\cdot\frac{1}{\sqrt{4kp_2}}\cdot\Pi(p_1-p_{45},M_N,\Gamma_N)\cdot\Pi(p_{67}-p_2,M_W,0)\cdot\hat{A}_\lambda^4+(45\leftrightarrow 67), \tag{A4}$$

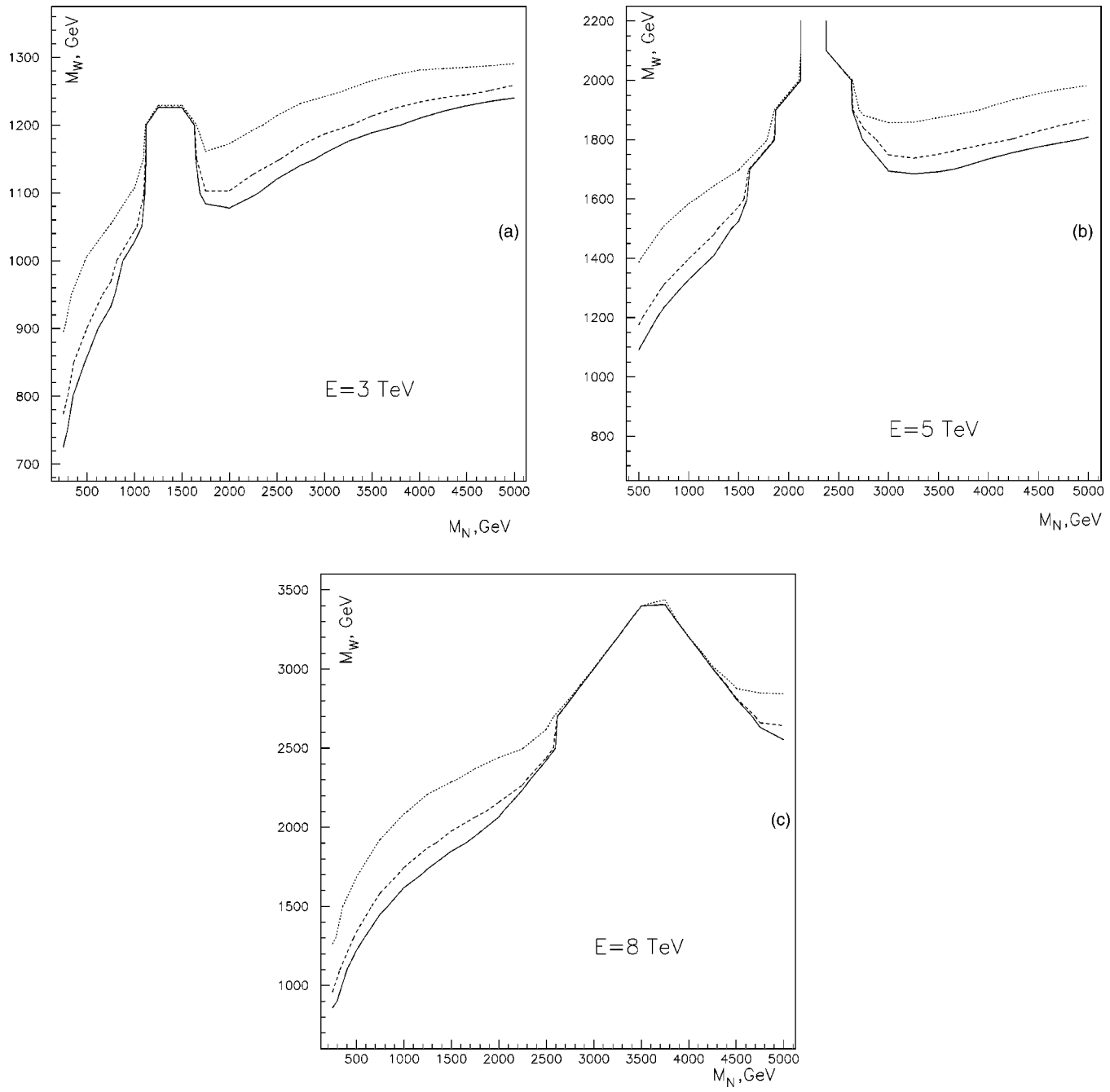

FIG. 7. The contour levels in the M_N–M_{W_R} plane that correspond to 99% (solid line), 95% (long-dashed line), and 63% (short-dashed line) probability of the discovery level (4.6, 3, and 1 event) for $\sqrt{s_{ee}}=3$ (a), 5 (b), and 8 (c) TeV. $M_{\Delta++}=600$ GeV.

$$\hat{A}_L^4 = -8M_N s(p_1,p_4)\{-t(p_5,p_7)s(p_6,p_3)[t(p_2,p_6)s(p_6,k)+t(p_2,p_7)s(p_7,k)]-s(p_6,p_2)t(p_2,p_7)t(p_5,p_2)s(k,p_3)$$
$$+t(p_5,p_2)s(p_2,p_3)s(p_6,k)t(p2,p7)\},$$

$$\hat{A}_R^4 = -8M_N s(p_1,p_4)\{-t(p_5,p_7)s(p_6,p_3)[s(p_2,p_6)t(p_6,k)+s(p_2,p_7)t(p_7,k)]-s(p_6,p_2)t(p_2,p_7)t(p_5,k)s(p_2,p_3)$$
$$+t(p_5,p_2)s(p_2,p_3)s(p_6,p_2)t(k,p7)\}.$$

$$A_\lambda^5 = \frac{ieg_R^2}{2}\cdot\frac{1}{\sqrt{4kp_2}}\cdot\Pi(p_1+p_2,0,0)\cdot\Pi(p_{45}+p_{67},M_\Delta,\Gamma_\Delta)\cdot\hat{A}_\lambda^5, \tag{A5}$$

$$\hat{A}_L^5 = 8M_N s(p_1,k)t(p_2,p_1)s(p_1,p_3)s(p_4,p_6)t(p_7,p_5),$$

$$A_R^5 = 8M_N s(p_1,p_2)[t(k,p_1)s(p_1,p_3)+t(k,p_2)s(p_2,p_3)]s(p_4,p_6)t(p_7,p_5).$$

$$A_\lambda^6 = \frac{ieg_R^2}{2}\cdot\frac{1}{\sqrt{4kp_2}}\cdot\Pi(p_3-p_2,0,0)\cdot\Pi(p_{45}+p_{67},M_\Delta,\Gamma_\Delta)\cdot A_\lambda^6, \tag{A6}$$

$$A_L^6 = -8M_N s(p_4,p_6)t(p_7,p_5)s(p_1,p_3)t(p_3,p_2)s(k,p_3),$$

$$\hat{A}_R^6 = -8M_N s(p_4,p_6)t(p_7,p_5)[s(p_1,p_3)t(p_3,k)-s(p_1,p_2)t(p_2,k)]s(p_2,p_3).$$

$$A_\lambda^7 = \frac{ieg_R^2}{2}\cdot\frac{1}{\sqrt{4kp_2}}\cdot\Pi(p_1-p_3,M_\Delta,\Gamma_\Delta)\cdot\Pi(p_{45}-p_2,M_W,0)\cdot\hat{A}_\lambda^7, \tag{A7}$$

$$\begin{aligned}\hat{A}_L^7 = &-8M_N s(p_1,p_3)\{s(p_4,k)t(p_2,p_5)s(p_6,p_2)t(p_2,p_7)-s(p_6,k)t(p_2,p_7)s(p_4,p_2)t(p_2,p_5)\\ &-[t(p_2,p_4)s(p_4,k)+t(p_2,p_5)s(p_5,k)]s(p_6,p_4)t(p_5,p_7)\},\end{aligned}$$

$$\begin{aligned}\hat{A}_R^7 = &-8M_N s(p_1,p_3)\{s(p_4,p_2)t(k,p_5)s(p_6,p_2)t(p_2,p_7)-s(p_6,p_2)t(k,p_7)s(p_4,p_2)t(p_2,p_5)\\ &-[s(p_2,p_4)t(p_4,k)+s(p_2,p_5)t(p_5,k)]s(p_6,p_4)t(p_5,p_7)\}.\end{aligned}$$

$$A_\lambda^8 = A_\lambda^7(p_4\leftrightarrow p_6, p_5\leftrightarrow p_7). \tag{A8}$$

$$A_\lambda^9 = \frac{ieg_R^2}{2}\cdot\frac{1}{\sqrt{4kp_2}}\cdot\Pi(p_1-p_3,M_\Delta,\Gamma_\Delta)\cdot\Pi(p_{45}+p_{67},M_\Delta,\Gamma_\Delta)\cdot\hat{A}_\lambda^9, \tag{A9}$$

$$\hat{A}_L^9 = 16M_N[t(p_2,p_1)s(p_1,k)-t(p_2,p_3)s(p_3,k)]s(p_1,p_3)s(p_4,p_6)t(p_7,p_5),$$

$$\hat{A}_R^9 = 16M_N[s(p_2,p_1)t(p_1,k)-s(p_2,p_3)t(p_3,k)]s(p_1,p_3)s(p_4,p_6)t(p_7,p_5).$$

[1] M. Gell-Mann, P. Ramond, and R. Slansky, in *Supergravity*, edited by P. van Nieuwenhuizen and D. Z. Friedman (North-Holland, Amsterdam, 1979); T. Yanadiga, in *Proceedings of Workshop on Unified Theories and Baryon Number in the Universe*, edited by O. Sawada and A. Sugamoto (KEK, Tsukuba, 1979); R.N. Mohapatra and G. Senjanovich, Phys. Rev. Lett. **44**, 912 (1980).

[2] G.B. Gelmini and M. Roncadelli, Phys. Lett. **99B**, 411 (1981).

[3] J.C. Pati and A. Salam, Phys. Rev. D **10**, 275 (1974); R.N. Mohapatra and J.C. Pati, *ibid.* **11**, 566 (1975); **11**, 2558 (1975); G. Senjanovich and R.N. Mohapatra, *ibid.* **12**, 1502 (1975); R.N. Mohapatra and R.E. Marshak, Phys. Lett. **91B**, 202 (1980); R.N. Mohapatra and D. Sidhu, Phys. Rev. Lett. **38**, 667 (1977).

[4] A. Ali, A. Borisov, and N. Zamorin, Eur. Phys. J. C **21**, 123 (2001); hep-ph/0112043; F. Almeida *et al.*, Phys. Lett. B **400**, 331 (1997); A. Ferrari *et al.*, Phys. Rev. D **62**, 013001 (2000).

[5] G. Cvetic, C.S. Kim, and C.W. Kim, Phys. Rev. Lett. **82**, 4761 (1999), and references therein; J. Maalampi, K. Mursula, and R. Vuorionpera, Nucl. Phys. **B372**, 23 (1992); W. Buchmuller and C. Greub, *ibid.* **B363**, 345 (1991); **B381**, 109 (1992).

[6] D. London, G. Belanger, and J. Ng, Phys. Lett. B **188**, 155 (1987); J. Maalampi, A. Pietila, and J. Vuori, Nucl. Phys. **B381**, 544 (1992); Phys. Lett. B **297**, 327 (1992); J. Maalampi and A. Pietila, Z. Phys. C **59**, 257 (1993); P. Helde, K. Huitu, J. Maalampi, and M. Raidal, Nucl. Phys. **B437**, 305 (1995); A. Pietila and J. Maalampi, Phys. Rev. D **52**, 1386 (1995); T. Rizzo, *ibid.* **50**, 5602 (1994); J. Maalampi and N. Romanenko, *ibid.* **60**, 055002 (1999).

[7] M. Flanz, W. Rodejohann, and K. Zuber, Phys. Lett. B **473**, 324 (2000).

[8] F. Almeida *et al.*, hep-ph/0201032.

[9] J. Peressutti, O.A. Sampayo, and J.I. Aranda, Phys. Rev. D **64**, 073007 (2001).

[10] L. Baudis *et al.*, Phys. Rev. Lett. **83**, 41 (1999); H.V. Kladpor-Kleingrothaus and H. Pas, hep-ph/0002109; M. Hirsh, H.V. Kladpor-Kleingrothaus, and O. Panella, Phys. Lett. B **374**, 7 (1996).

[11] Parallel Data Group, K. Hagiwara *et al.*, Phys. Rev. D **66**, 010001 (2002).

[12] CLIC Study Team, R. W. Assmann *et al.*, "A 3-TeV e^+e^- Linear Collider Based on CLIC Technology," edited by G. Guignard, CERN 2000-08; M. Battaglia, CLIC Note 474 LC-PHSM-2001-072-CLIC, 2001; A. De Roeck (private communication).

[13] S. Godfrey, P. Kalyniak, and N. Romanenko, Phys. Rev. D **65**, 033009 (2002).

[14] J.F. Gunion, J. Grifols, A. Mendez, B. Kayzer, and F. Olness, Phys. Rev. D **40**, 1546 (1989).

[15] R. Kleiss and W.J. Stirling, Nucl. Phys. **B262**, 235 (1985).

[16] P.A. Baikov *et al.*, ''Physical Results by Means of CompHEP,'' in *Proceedings of the Xth International Workshop on High Energy Physics and Quantum Field Theory (QFTHEP-95)*, Zvenigorod, Russia, 1995, edited by B. Levtchenko and V. Savrin (Moscow University Press, Moscow, 1996), p. 101, hep-ph/9701412; E.E. Boos, M.N. Dubinin, V.A. Ilyin, A.E. Pukhov, and V.I. Savrin, hep-ph/9503280.

[17] I.F. Ginzburg *et al.*, Nucl. Instrum. Methods Phys. Res. **205**, 47 (1983); **219**, 5 (1984); V.I. Telnov, Nucl. Instrum. Methods Phys. Res. A **294**, 72 (1990); C. Akerlof, Report No. UM-HE-81-59.

[18] R. Hemingway, *Proceedings of the 16th Lake Louise Winter Institute*, Lake Louise, Alberta, Canada, 2001, edited by A. Astbury, B.A. Campbell, F.C. Khanna, and M.G. Vincter (World Scientific, Singapore, 2002), p. 1.